ELSEVIER

Spectrochimica Acta Part B 63 (2008) 277–286

SPECTROCHIMICA ACTA PART B

www.elsevier.com/locate/sab

Femtosecond laser ablation: Experimental study of the repetition rate influence on inductively coupled plasma mass spectrometry performance ☆

Jhanis J. Gonzalez [a], Alberto Fernandez [b], Dayana Oropeza [a], Xianglei Mao [a], Richard E. Russo [a,*]

[a] *Lawrence Berkeley National Laboratory, Berkeley, CA 94720, USA*

[b] *Centro de Fisicoquímica. Escuela de Química, Universidad Central de Venezuela, Caracas 1020-A, Venezuela*

Received 21 August 2007; accepted 23 November 2007

Abstract

This paper demonstrates the feasibility of performing bulk chemical analysis based on laser ablation for good lateral resolution with only nominal mass ablated per pulse. The influence of repetition rate (1–1000 Hz) and scan speed (1–200 μm/s) using a low energy (30 μJ) and a small spot size (~10 μm) UV-femtosecond laser beam was evaluated for chemical analysis of silica glass samples, based on laser ablation sampling and inductively coupled plasma mass spectrometry (ICP-MS). Accuracy to approximately 14% and precision of 6% relative standard deviation (RSD) were measured. Published by Elsevier B.V.

Keywords: LA-ICP-MS; Femtosecond LA-ICP-MS; Repetition rate effects

1. Introduction

Laser ablation sampling for inductively coupled plasma mass spectrometry (LA-ICP-MS) has become one of the most popular approaches for analysis of solid samples. When compared with conventional dissolution techniques, laser ablation offers direct characterization of solids, reduced risk of contamination and sample loss, analysis of very small samples not separable for solution analysis, rapid analysis, and spatial resolution. Chemical analysis using laser ablation is a straightforward process in which a high energy laser pulse is used to transform a portion of a solid sample into aerosol for subsequent chemical analysis. LA-ICP-MS can be divided into three stages, namely: laser–material interaction (stage 1); ablated mass transport (stage 2), and ICP digestion-detection (stage 3). These stages are interrelated since stage 1 will affect stage 2, and stage 2 will affect stage 3. However, each of these stages can be studied and optimized separately.

The laser–material interaction (stage 1) depends on several of the beam properties; among these are: pulse duration, energy,

Table 1
Experimental conditions

Laser ablation devices	Spectra Physics Mai Tai Ti:sapphire (150 fs) Energy=30 μJ Spot size on the sample=~10 μm Fluence=38 J/cm^2
ICP-MS	PQ3, VG-Elemental
Detector	Simultaneous mode detector
ICP-MS parameters	
RF power	1350 V
Plasma Ar gas flow rate	14.2 L/min
Auxiliary Ar gas flow rate	1.02 L/min
Carrier (Ar) flow rate	1.25 L/min
ICP-MS dwell time	10 ms
Isotopes	^{7}Li, ^{43}Ca, ^{55}Mn, ^{59}Co, ^{88}Sr, ^{115}In, ^{139}La, ^{208}Pb, ^{232}Th, ^{238}U
Data acquisition mode	Time resolved (TRA)

☆ This article is published in a special honor issue dedicated to Jim Winefordner on the occasion of his retirement, in recognition of his outstanding accomplishments in analytical atomic and molecular spectroscopy. R. Russo extends an additional appreciation to Professor Winefordner for introducing him to analytical laser spectroscopy as an undergraduate chemistry student.

* Corresponding author. Tel.: +1 510 486 4258; fax: +1 510 483 7303.
E-mail address: RERusso@lbl.gov (R.E. Russo).

0584-8547/$ - see front matter. Published by Elsevier B.V.
doi:10.1016/j.sab.2007.11.035

Table 2
Compositions of the reference standard series NIST 610–616

Element concentration (ppm)		
	610	612
Li	484.6±21.7 [a]	41.54±2.87 [a]
Co	405±22.9 [a]	35.26±2.44 [a]
La	457.4±72.4 [a]	35.77±2.15 [a]
Pb	426±1 [b]	38.57±0.2 [b]
Th	457.2±1.2 [b]	37.79±0.08 [b]
U	461.5±1.1 [b]	37.38±0.08 [b]
[U/Th]	1.009	0.989

[a] From Pearce N.J.G. et al. Geostandards Newsletter. 1997.21. 115–144.
[b] Certified concentration (NIST).

wavelength, spatial energy profile, fluence, and repetition rate. These parameters play a dominant role in defining the quantity and chemistry of the ablated aerosol. The influence of these properties has been well documented for nanosecond laser ablation [9,14], and only investigated recently for femtosecond laser ablation chemical analysis. Research into femtosecond laser ablation is based on improved performance expectations by controlling the amount of ablated material, particle size distribution, matrix dependence, and fractionation. Femtosecond laser ablation sampling into the ICP-MS has been shown to provide good chemical analysis precision and accuracy by reducing systematic errors related to the particle size distribution and resultant spikes in the ICP-MS response [4,5,10]. A relaxation of matrix dependence also has been shown for the analysis of glass and metal alloy samples when using femtosecond laser pulses [1,2,5,8,10].

In this work, the influence of repetition rate and scan speed using low energy (~30 μJ) UV-femtosecond laser pulses on the particle size distribution and LA-ICP-MS performance (accuracy and precision) was studied. Crater profiles also were investigated for two silica glass samples (NIST 610 and 612).

2. Experimental

The experimental system included a femtosecond laser consisting of a Spectra Physics Mai Tai Ti:sapphire seed laser and Spitfire regenerative amplifier. The 150 fs pulses at 800 nm were frequency tripled to obtain the 266-nm wavelength. An ICP-MS (PQ3 from VG Elemental) was used to chemically analyze the ablated mass and a SMPS (Scanning Mobility Particle System, TSI incorporated) 3936 series system was used for particle size measurements.

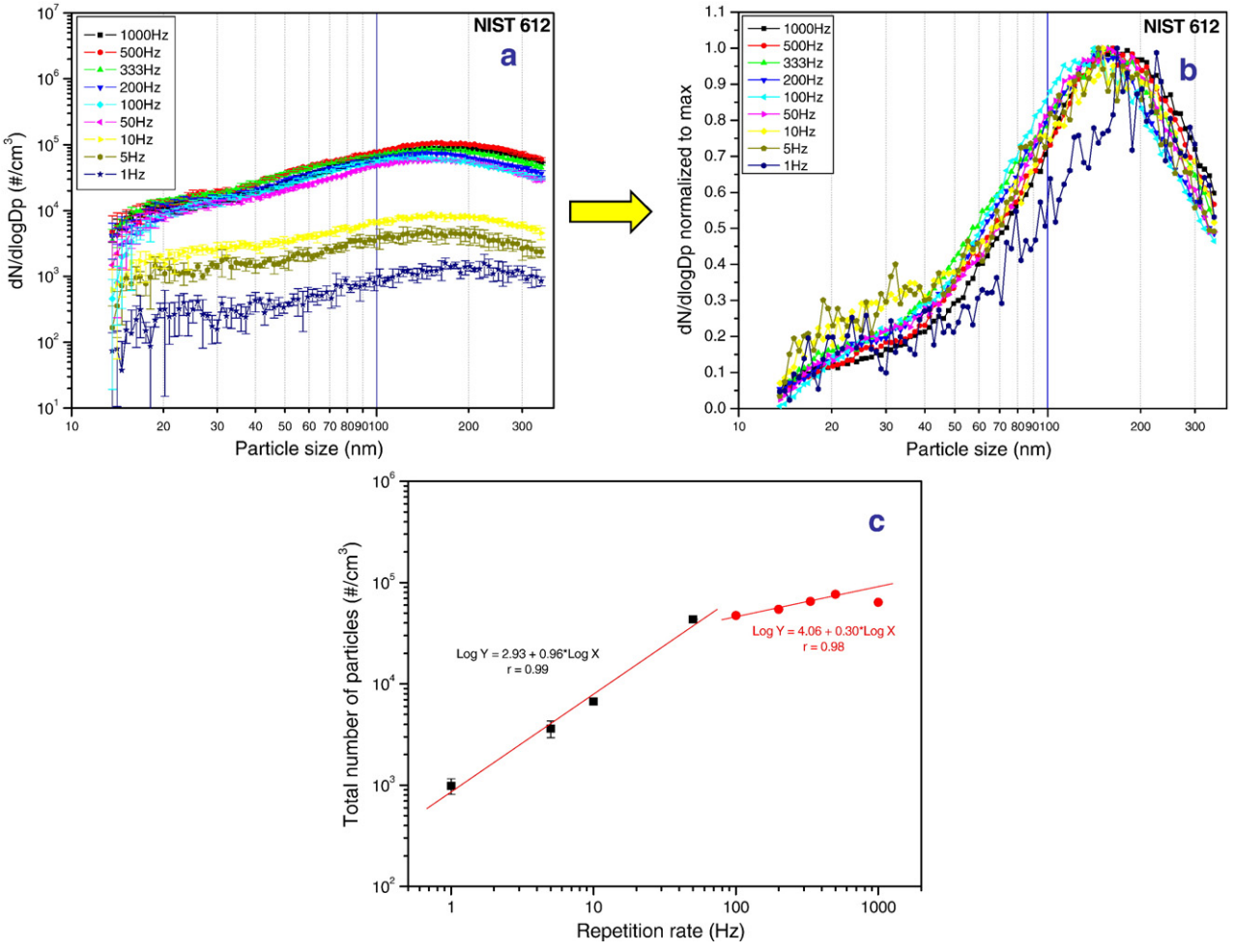

Fig. 1. NIST 612 particle size distribution (SMPS) at different pulse repetition rates. a) Number density of particles. b) Number density of particles normalized to maximum. c) Total number of particle versus repetition rate.

Laser ablation was performed in an argon environment under atmospheric pressure. For the particle size distribution measurements, a flow switch was installed before the inlet to the SMPS to ensure the working flow rate of 0.3 L/min; the remainder of the flow was discarded through a filter. Table 1 shows the experimental conditions.

Silica glasses from the National Institute of Standards and Technology (NIST 610 and 612) having a common matrix (SiO_2, CaO, Na_2O, and Al_2O_3) were used as samples in this work. The concentrations of lithium, cobalt, lanthanum, lead, thorium and uranium (Table 2) in NIST 612 glass (transparent sample) were determined by using NIST 610 (opaque sample) as a calibration standard and calcium (^{43}Ca) as an internal standard.

3. Results and discussion

3.1. Qualitative study

Most particle size distribution functions can be described using the following parameters: *number density*, *particle diameter and span*. *Number density:* when using the differential mobility analyzer (DMA) system the primary measurement is the differential number concentration (dN) of the aerosol per unit volume of gas sampled, which is the concentration of particles in a given channel. The DMA system is sensitive to the number of particles in the aerosol sample as opposed to particle mass, color, shape composition or other characteristics. The normalized number concentration, dN/dlogDp, is calculated by dividing dN by the geometric width of the size channel. This normalized concentration format allows particle size distributions to be compared regardless of the channel resolution.

Particle size distributions for different laser pulse repetition rates with a fixed sample scan speed of 10 μm/s are shown in Fig. 1; Fig. 1a shows the number density versus particle size and Fig. 1b shows the number density of particles normalized to the maximum value. The distribution functions show little change when increasing the repetition rate from 1 to 1000 Hz at this sample scan speed. The number density of particles increases when the repetition rate increased from 1 to 50 Hz and then the slope decreases by a factor of ~3 after 100 Hz (Fig. 1c). The steep increase in the number density of particles between 1 and 50 Hz is due to an increased amount of ablated mass. As can be seen in Fig. 2, the crater profiles measured with a white light interferometric microscope (Zygo, New View 200) show an analogous behavior to the number density of particles in which there is a steep increase in the crater depth between 1 and 50 Hz; a slower increase in the crater depth is manifested at higher repetition rates.

A rim forms around the craters at repetition rates greater than 50 Hz; Fig. 3 shows the crater profile at each repetition rate using a white light interferometric microscope. Rim growth indicates that there is a heat accumulation effect from

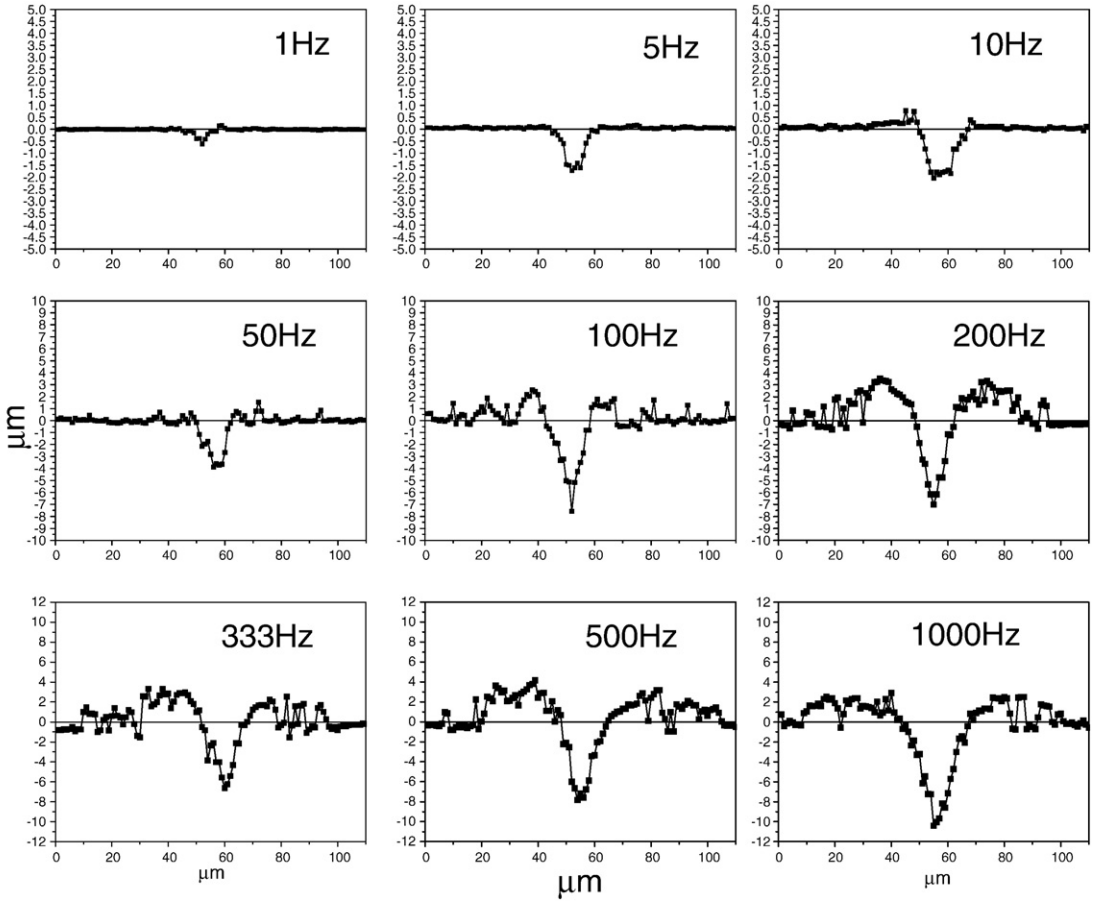

Fig. 2. NIST 612 crater profiles generated at different laser repetition rates. Scan speed 10 μm/s.

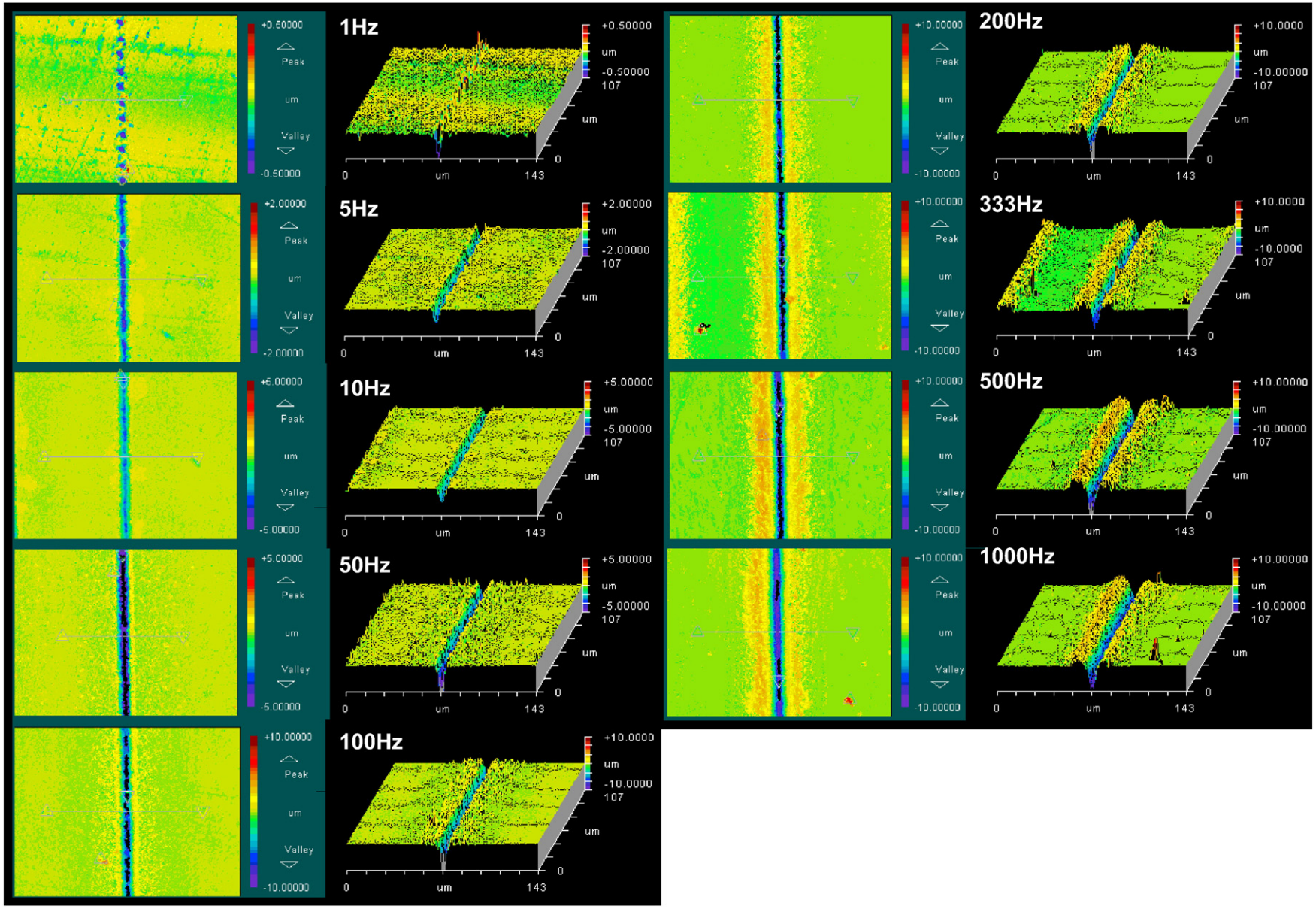

Fig. 3. NIST 612 interferometric images of ablation craters generated at different laser repetition rates. Scan speed 10 μm/s.

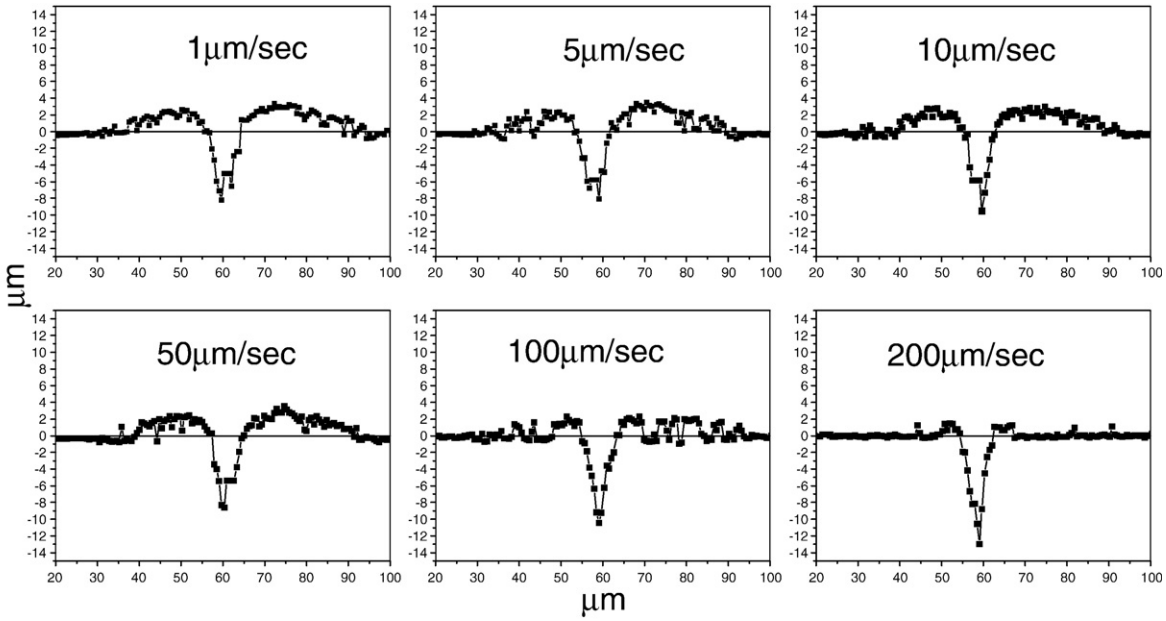

Fig. 4. NIST 612 crater profiles generated at different scan speeds.

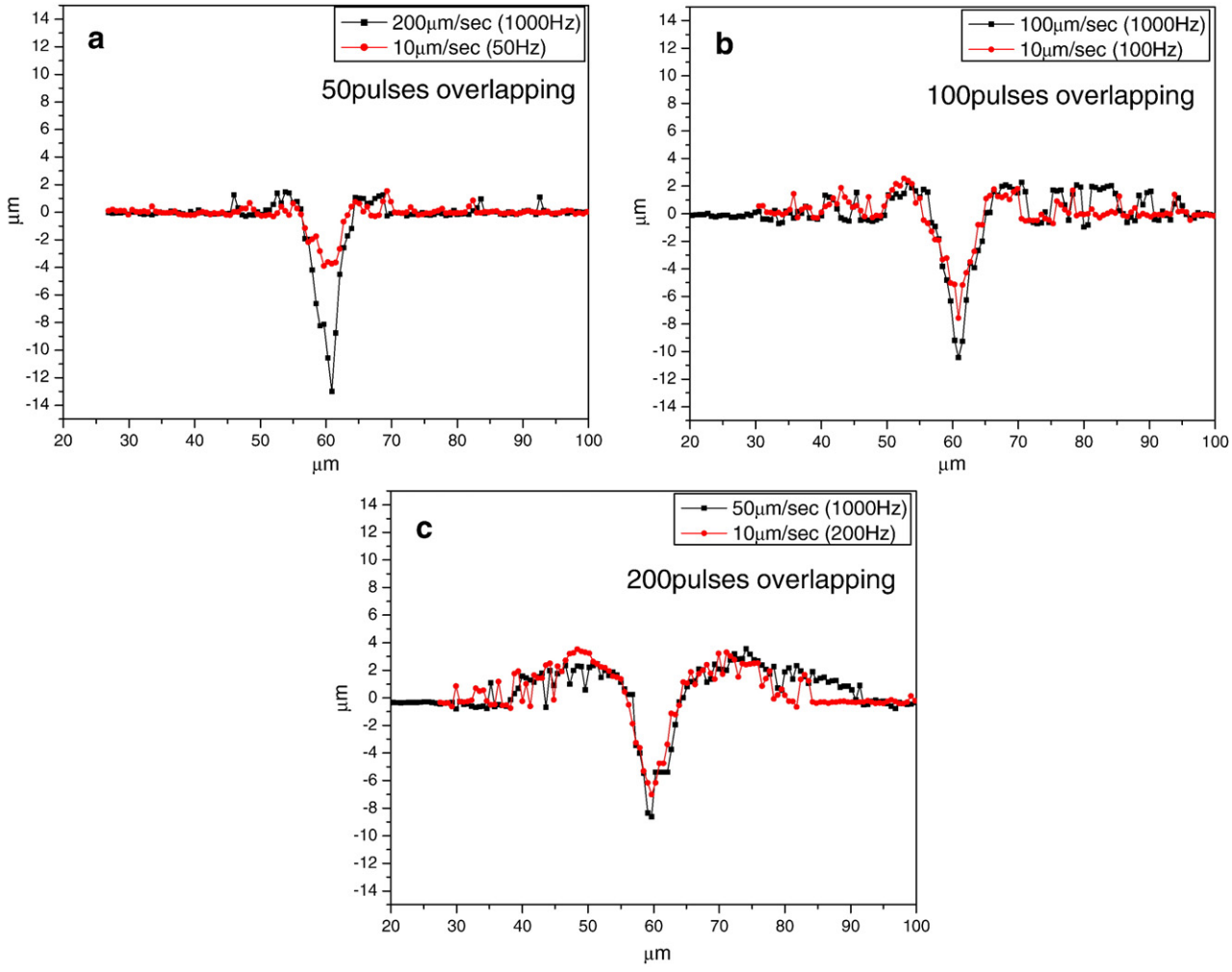

Fig. 5. NIST 612 comparisons of crater profiles with different numbers of pulses overlapping by changing repetition rate or scan speed. a) 50 pulses, b) 100 pulses, and c) 200 pulses overlapping.

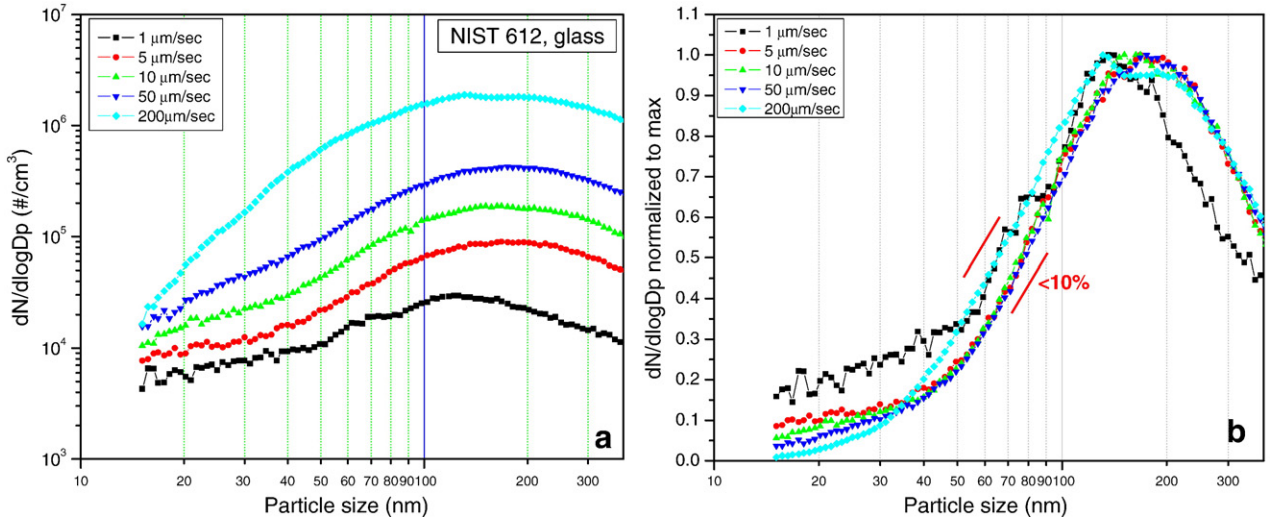

Fig. 6. NIST 612 particle size distribution (SMPS) at different scan speeds. a) Number density of particles. b) Number density of particles normalized to maximum.

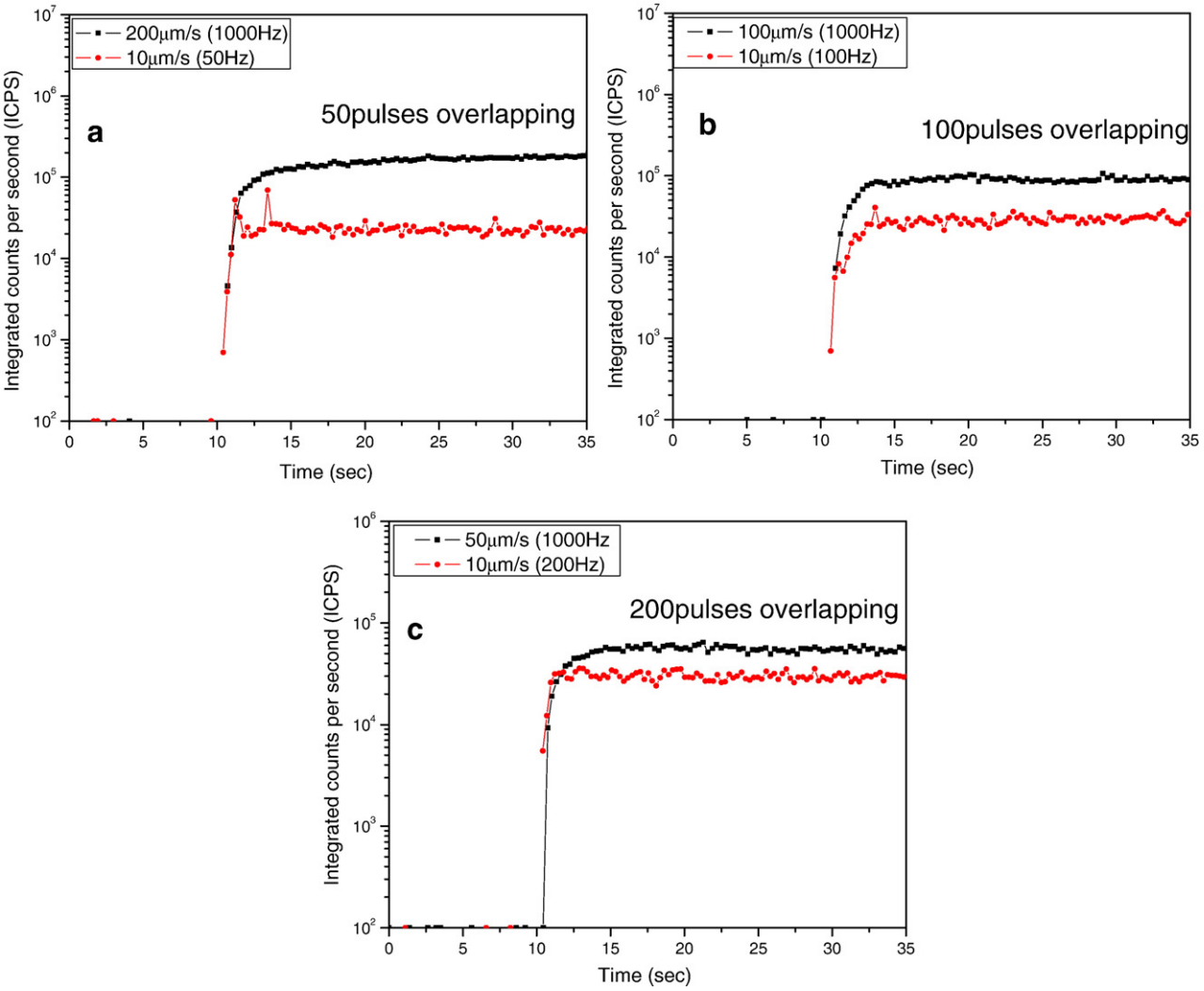

Fig. 7. ^{115}In integrated counts per second (ICPS) from NIST 612. Comparisons of ICP-MS signals with different numbers of pulses overlapping by changing repetition rate or scan speed. a) 50 pulses, b) 100 pulses, and c) 200 pulses overlapping.

overlapping laser pulses in the same sample area. In these experiments with increasing repetition rate at fixed scan speed (10 μm/s), the only parameter changing is the number of overlapping laser pulses. The number of overlapping pulses was calculated using the beam spot size (10 μm), the scan speed (10 μm/s), and the repetition rate (Hz). For example, at the point when the slope of the total concentration of particles changes (50 Hz), there are 50 laser pulses overlapping; and for 1 Hz there is only one pulse per position (10 μm/s). To test that pulse overlap is causing a heat accumulation effect, the repetition rate was fixed at 1000 Hz and the scan speed was varied from 1 to 200 μm/s (Fig. 4). The crater rim was reduced when the scan speed was increased (decreasing the number of overlapping pulses) until it disappeared at 200 μm/s.

Comparison of the different approaches for overlapping pulses is presented in Fig. 5. It can be seen that at 50 (Fig. 5a), 100 (Fig. 5b), and 200 (Fig. 5c) overlapping pulses, the results were similar in term of the rim formation; no matter the approach used to produce the overlap. However, when 50 pulses overlapped (Fig. 5a), there was a difference in the crater depth; the crater was deeper at a combination of the highest scan speed and repetition rate (200 μm/s and 1000 Hz). One possible explanation is that the highest scan speed of 200 μm/s avoided the effect of particles accumulating in front of the sample and/or within the trench causing shielding. Thus there was a more efficient coupling of the incoming beam to the sample, resulting in additional ablated mass.

Particle size distribution measurements also were completed for this approach (Fig. 6). Similar to the data when the scan speed was fixed (10 μm/s), there was no significant systematic difference between the distribution functions (<10%). However, there was an increased amount of particles reaching the SMPS as well as an increased ICP-MS signal when using the fastest scan speed of 200 μm/s (fewest overlapping pulses 50). Fig. 7 shows ICP-MS signals for the two approaches of pulse overlapping. It is noticeable that even though the particle size distribution function does not change significantly, the higher speed and fixed repetition rate produce stronger signals compared to the fixed low speed. The differences in ablation or/and transport efficiency at different combinations of scan speeds and repetition rates could be the effect of absorption/diffusion of the laser beam by particles accumulated in front of the sample surface and/or particles trap inside the trench. To address this hypothesis, the influence of carrier gas flow rate on the particle size distribution was evaluated. Fig. 8 shows interferometric images of the craters generated using a scan speed of 10 μm/s and repetition rate of 1000 Hz when the carrier gas (argon) flow rate was varied. The argon flow rate did not significantly influence the formation of the crater rim. However, the flow rate affects the particle size distribution, shifting the

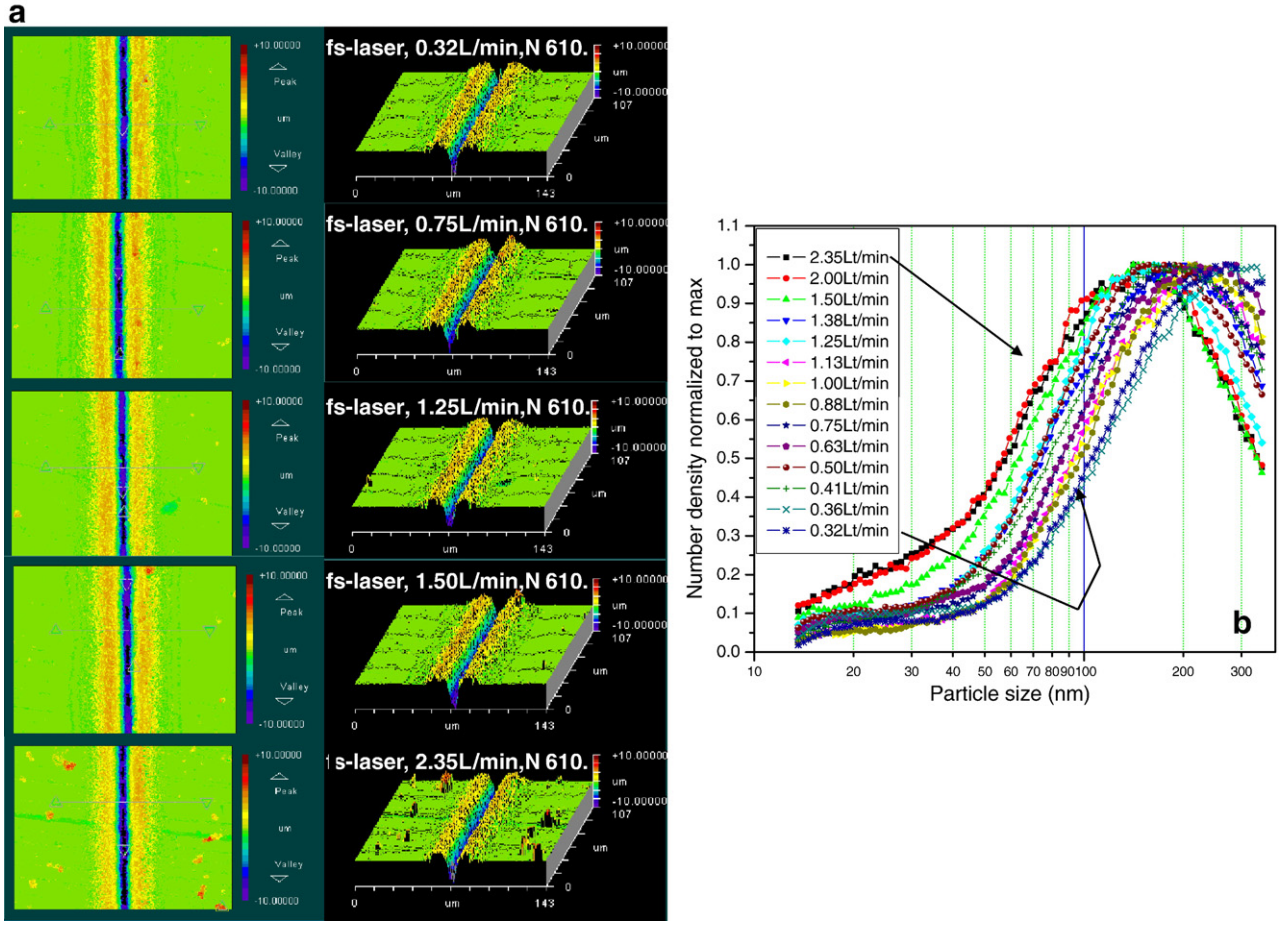

Fig. 8. a) NIST 612 interferometric images of the ablation craters generated under different Ar flow rates. b) Number density of particles normalized to maximum.

distribution to larger sizes with decreasing flow rate (Fig. 8b). As has been reported in studies of particle formation by flame aerosol reactors [12,13,15,16] the particle size strongly depends on the residence time in the flame; longer residence times prolongs particle coalescence increasing the primary particle size. As a parallelism to the laser ablation case, low gas flow rates increase the transport time between the ablation chamber and the detection system, increasing the collision time and agglomeration of particles.

3.2. Quantitative study

The ICP-MS response was monitored when varying the scan speed at fixed repetition rate (1000 Hz). Fig. 9 shows that the ICP-MS response of a matrix element ^{43}Ca (a) and a trace element ^{115}In (b) increased with the scan speed. This behavior was similar to that measured for the number density of particles with the SMPS. Therefore, the low ICP-MS response at low scan speed also could be attributed to the accumulation of particles in front of the surface, decreasing the ablation and/or transport efficiency due to the absorption/diffusion of the laser beam as reported by Brygo et al. [3].

At a scan speed of 200 μm/s, rim formation was minimum and the ICP-MS response was greatest; all studies of analytical performance were conducted at 1000 Hz and 200 μm/s. The analytical performance of the low energy (μJ) UV-femtosecond laser (accuracy and precision) was evaluated by performing bulk analysis of NIST 612 ("unknown" sample) and NIST 610 as standard sample with ^{43}Ca as internal standard (as in a previous report [6]).

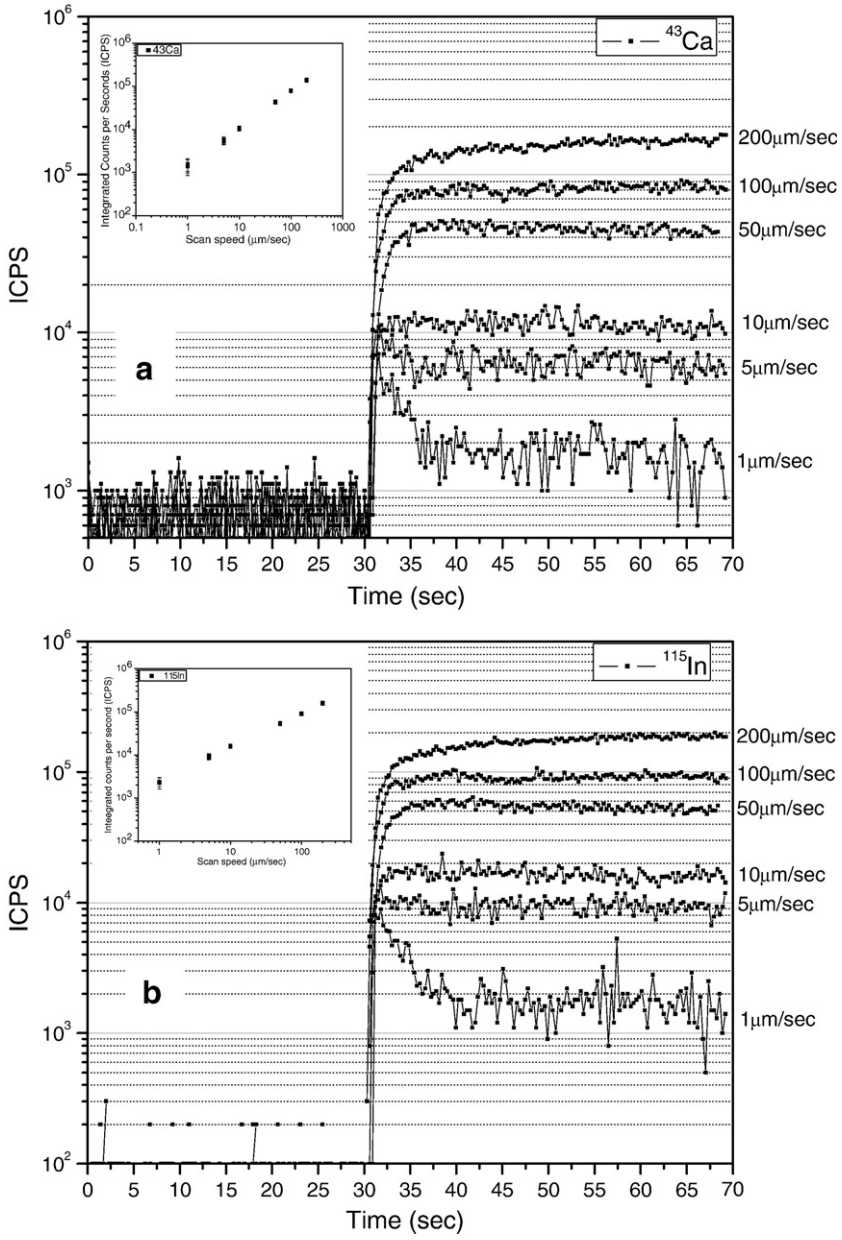

Fig. 9. ICP-MS signals at different scan speeds.

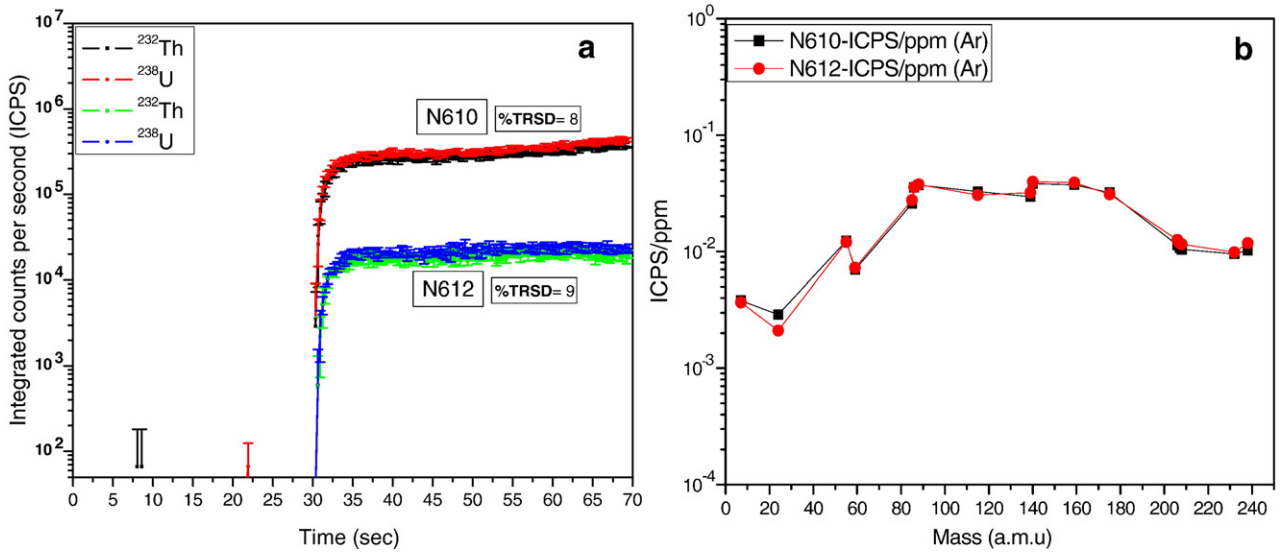

Fig. 10. NIST 610–612: a) ^{232}Th and ^{238}U ICP-MS signal. b) ICP-MS response curves.

Fig. 10a shows the ^{232}Th and ^{238}U response from NIST 610 and 612 and the temporal relative standard deviation (TRSD) as a measure of the transient signal precision [7]. The TRSD is very similar for both samples even though the difference in concentration was about ~10 times NIST 610/NIST 612. For ICP-MS chemical analysis (liquid nebulization or laser ablation), the accuracy of the measurements will depend on the closeness of the response curves between the "unknown" sample (NIST 612) and the "standard" (NIST 610); the closer the response curves more accurate the analysis. Fig. 10b shows the closeness of the response curve normalized to the internal standard for these two samples. Table 3 shows that the average concentrations under the conditions in this study (~10 μm spot size, 1000 Hz and 200 μm/s) were very accurate and agree with the values reported in the literature [11]. These data demonstrate the feasibility of performing bulk chemical analysis with a small spot size for good lateral resolution and good analytical performance.

4. Summary

The combination of spot size ~10 μm, repetition rate of 1000 Hz, and scan speed of 200 μm/s can be successfully used for bulk analysis of glass samples with good lateral resolution. At low repetition rates (<100 Hz) with fixed scan speed (10 μm/s), there was a linear increase in the crater depth, with much slower increase (~1/3) at higher repetition rates (>100 Hz). For particular combinations of scan speed and repetition rates, a heat accumulation effect in the samples led to the formation of a rim surrounding the crater. Accumulation of particles in front of the sample surface may absorb or diffuse the incident laser beam, reducing the coupling efficiency and decreasing particle transport efficiency.

Table 3
Measured concentration for selected elements in NIST 612 using NIST 610 as a standard and calcium (^{43}Ca response) as internal standard

Ar-fs-1000 Hz	Average		SD	%RSD	%Accuracy
Li	40	±	1	2	−3
Co	37	±	1	3	5
La	41	±	1	3	14
Pb	42	±	1	3	10
Th	38	±	2	6	−0.03
U	40	±	2	6	6
Th/U	0.96	±	0.01	1	−3

Concentrations in ppm (μ/g).

Acknowledgements

We would like to thank Paul Berdahl for productive discussions and for editing the manuscript. This work was supported by the Office of Science, Office of Basic Energy Sciences, Chemical Sciences, Geosciences, and Biosciences Division, and the Deputy Administrator for Defense Nuclear Nonproliferation, Research and Development of the U.S. Department of Energy under Contract No. DE-AC02-05CH11231.

References

[1] Q.Z. Bian, C.C. Garcia, J. Koch, K. Niemax, Non-matrix matched calibration of major and minor concentrations of Zn and Cu in brass, aluminium and silicate glass using NIR femtosecond laser ablation inductively coupled plasma mass spectrometry, J. Anal. At. Spectrom. 21 (2006) 187–191.
[2] Q.Z. Bian, J. Koch, H. Lindner, H. Berndt, R. Hergenroder, K. Niemax, Non-matrix matched calibration using near-IR femtosecond laser ablation coupled plasma optical emission spectrometry, J. Anal. At. Spectrom. 20 (2005) 736–740.
[3] F. Brygo, Ch. Dutouquet, F. Le Guern, R. Oltra, A. Semerok, J.M. Weulersse, Laser fluence, repetition rate and pulse duration effects on paint ablation, Appl. Surf. Sci. 252 (2006) 2131–2138.
[4] C.C. Garcia, H. Lindner, K. Niemax, Transport efficiency in femtosecond laser ablation inductively coupled plasma mass spectrometry applying ablation cells with short and long washout times, Spectrochim. Acta Part B 62 (2007) 13–19.

[5] J. Gonzalez, S.H. Dundas, C. Liu, X.L. Mao, R.E. Russo, UV-femtosecond and nanosecond laser ablation-ICP-MS: internal and external reproducibility, J. Anal. At. Spectrom. 21 (2005) 778–784.
[6] J. Gonzalez, S.H. Dundas, C. Liu, X.L. Mao, R.E. Russo, UV-femtosecond and nanosecond laser ablation-ICP-MS: internal and external reproducibility, J. Anal. At. Spectrom. 21 (2006) 778–784.
[7] J. Gonzalez, A. Fernandez, X.L. Mao, R.E. Russo, Scanning vs. single spot laser ablation (213 nm) inductively coupled plasma mass spectrometry, Spectrochim. Acta Part B 59 (2004) 369–374.
[8] J. Gonzalez, C.Y. Liu, X.L. Mao, R.E. Russo, UV-femtosecond laser ablation-ICP-MS for analysis of alloys samples, J. Anal. At. Spectrom. 19 (2004) 1165–1168.
[9] D. Günther, I. Horn, B. Hattendorf, Recent trends and developments in laser ablation-ICP-mass spectrometry, Fresenius J. Anal. Chem. 368 (2000) 4–14.
[10] C. Liu, X.L. Mao, S.S. Mao, X. Zeng, R. Greif, R.E. Russo, Nanosecond and femtosecond laser ablation of brass: Particulate and ICPMS measurements, Anal. Chem. 76 (1-15-2004) 379–383.
[11] N.J.G. Pearce, W.T. Perkins, J.A. Westgate, M.P. Gorton, S.E. Jackson, C.R. Neal, S.P. Chenery, A compilation of new and published major and trace element data for NIST SRM 610 and NIST SRM 612 glass reference materials. Geostandards Newsletter. The Journal of Geostandards and Geoanalysis 21(1997). 115–144.
[12] S.E. Pratsinis, Flame aerosol synthesis of ceramic powders, Pror. Energy Combust. Sci. 24 (1998) 197–219.
[13] S.E. Pratsinis, S. Vemury, Particle formation in gases: a review, Powder Technol. 88 (1996) 267–273.
[14] R.E. Russo, X.L. Mao, H.C. Liu, J. Gonzalez, S.S. Mao, Laser ablation in analytical chemistry — a review, Talanta 57 (2002) 425–451.
[15] T. Tani, K. Takatori, S.E. Pratsinis, Evolution of the morphology of zinc oxide/silica particles made by spray combustion, J. Am. Ceram. Soc. 87 (2004) 365–370.
[16] S. Tsantilis, S.E. Pratsinis, Soft- and hard-agglomerate aerosols made at high temperatures, Langmuir 20 (2004) 5933–5939.